PAPER • **OPEN ACCESS**

Comparative study on structural, electronic, optical and mechanical properties of normal and high pressure phases titanium dioxide using DFT

To cite this article: Neerja Dharmale *et al* 2020 *Mater. Res. Express* **7** 054004

Materials Research Express

PAPER

Comparative study on structural, electronic, optical and mechanical properties of normal and high pressure phases titanium dioxide using DFT

Neerja Dharmale[1], **Saurabh Chaudhury**[1], **Rupesh Mahamune**[2] and **Debashish Dash**[3]

[1] Department of Electrical Engineering, National Institute of Technology, Silchar, Assam 788010, India
[2] Department of Electronic and Instrumentation, National Institute of Technology, Silchar, Assam 788010, India
[3] Department of Electronics and Communication Engineering, Madanapalle Institute of Technology and Science, Andhra Pradesh 517325, India

E-mail: neerja.rupesh@gmail.com

Keywords: mechanical properties, electronic properties, structural properties, optical properties, elastic constants, effective mass, density functional theory

OPEN ACCESS

RECEIVED
11 March 2020

REVISED
15 April 2020

ACCEPTED FOR PUBLICATION
27 April 2020

PUBLISHED
11 May 2020

Abstract

In this paper, a Self-consistent Orthogonalized linear combination of atomic orbitals (OLCAO) technique with a generalized gradient approximation such as Perdew–Burke–Ernzerhof Solid (GGA-PBE SOL) has been used to scrutinize the structural, optical, electronic and mechanical properties of normal pressure phase (Anatase and Rutile) and high pressure phase i.e., cubic (Fluorite and Pyrite) TiO_2. Electronic and optical properties of normal pressure phases of TiO_2 are also investigated using (Meta) MGGA-Tran and Blaha (TB09) and obtained results are a close approximation of experimental data. It is seen that the virtually synthesized structural parameter for cubic and tetragonal phases of TiO_2 are consistent with experimental and theoretical data. From the effective mass of charge carriers (m^*), it can be observed that pyrite TiO_2 is having lower effective mass than the fluorite and hence shows higher photocatalytic activity than fluorite. Furthermore, it is seen that fluorite is more dense than anatase, rutile and pyrite TiO_2. From the theoretical calculations on the optical properties, it can be concluded that optical absorption occursin the near UV region for high and normal pressue phases of TiO_2. Again from the reflectivity characteristics $R(\omega)$, it can be concluded that TiO_2 can be used as a coating material. Elastic constants, elastic compliance constants, mechanical properties are obtained for anatase, rutile, fluorite and pyrite TiO_2. A comparison of the results with previously reported theoretical and experimental data shows that the calculated properties are in better agreement with the previously reported experimental and theoretical results.

1. Introduction

TiO_2 occurs in many different forms. The naturally occurring forms of TiO_2 are TiO_2-B(Bronze), brookite, anatase and rutile [1]. Other forms of TiO_2 are columbite [2], baddeleyite [3], cotunnite [4], pyrite, fluorite, Tridymite [5], hollandite [6] and bronze [7, 8]. TiO_2 is a promising candidate in applications such as, coatings solar cells, photocatalysis, white pigment, biogas sensors, energy storage, etc, [9–18]. Nanotubes [19], nanowire [20] made from TiO_2 with suitable doping, thin films [21] of rutile TiO_2 with PbO_2 coating are found to be suitable in Dye Sensitized Solar Cells (DSSC'S). Also, adsorption of hydroxamate onto anatase TiO_2 surfaces [22] increases electron transfer event with less time period. Hence, it is more appropriate for energy harvesting applications. Since last decade, high-pressure phase TiO_2 is gaining attention because of its unique properties which play an important role in various applications. Cubic TiO_2 is formed by heating anatase TiO_2 at a high temperature of about 1900–2100k under high pressure of about 48 GPa in a diamond anvil cell [23, 24]. Cubic TiO_2 is the best choice for solar photovoltaic applications to extract solar energy and a healthy choice for a hazard-free environment [25].

There exist several approaches to theoretically investigate the properties of this material such as local density approximation (LDA) and generalized gradient approximation (GGA), MGGA under the framework of DFT along with various exchange-correlation functional. Gong sai *et al* [26], used TB-mBJ (Tran-Blaha modified Becke-Johnson) potentialand obtained properties were in better agreement with the experimental results and considered to be much better compared to LDA and GGA approach. Zhi-Gang Mei *et al* [27], used LDA and GGA along with various exchange correlations for calculating structural, mechanical and phonon properties of rutile and anatase TiO_2 and found that GGA-PBES provide accurate structural and mechanical properties for both the phases. Samat *et al* [14], calculated structural, optical and electronic properties of brookite TiO_2 using GGA with various exchange-correlation and found that structural properties calculated using GGA-WC are in good agreement with experimental values than the remaining exchange-correlation. Shatendra Sharma *et al* [28], calculated the electronic and optical properties for Strontium Sulphide (SrS) using LDA, GGA, and MGGA and observed that MGGA gives the bandgap value more close to experimental value while LDA and GGA gives underestimated results. Dash *et al* [25, 29], used OLCAO- LDA- Perdew and Zunger (PZ) (1981) method to investigate various properties of anatase and cubic TiO_2 and found an improvement in mechanical properties. Coronado *et al* [30], also used OLCAO-GGA method to verify the experimental data with theoretical data.

Researchers have calculated the structural, elastic, electronic, optical, thermal and acoustic properties of various phases of TiO_2 theoretically [6, 23, 25, 26, 29, 31–38] as well as experimentally [11, 30, 39–42]. Zhang *et al* [43], analyzed the photocatalytic activity among natural phases of TiO_2 based on the comparison of effective masses for these polymorphs and found that anatase is having higher photocatalytic activity than other two polymorphs. Mattesini *et al* [44] and Mahmood *et al* [26], found that fluorite TiO_2 is having a more absorptive transition in the visible region compared to pyrite TiO_2. As fluorite and pyrite are having cubic symmetry, it has only one dielectric tensor whereas tetragonal phases are having two dielectric tensor [45].

From the literature, it reveals that all the properties of TiO_2 are sensitive to exchange correlation used. OLCAO is able to give effective improvement in terms of different elastic and mechanical properties rather than plane wave and other theoretical results. GGA-PBESOL provides better structural and mechanical properties than other exchange correlations. Hence, the first objective of this work is to carry outa detail analysis of the structural, electronic, optical and mechanical properties of high pressure and normal pressure phases of TiO_2 using OLCAO-GGA-PBES. Second objective is to provide a detail comparision of the obtained results of high pressure and normal pressure phases of TiO_2 with each other and with previously available experimental and theoretical data. However, GGA also causes overestimation of lattice constants and underestimation of bandgap value. Third objective is to get results consistent with experimental data.As experimental data is available for normal pressure phases of TiO_2, MGGA-TB09 [46] is used here for analyzing its electronic and optical properties. The last objective is to calculate the m^* of charge carriers for the cubic phase of TiO_2 to find its possible application in photo-catalytic activity and compared with other phases of TiO_2.

The rest of the paper is arranged as follows. Section 2 explains the adopted computational details for the analysis of all properties of TiO_2. Section 3 details the results and discussion on obtained properties. Finally, sections 4 and 5 gives the conclusion and future scope of the work.

2. Materials and methodology

Here, computations are carried out for anatase, rutile, fluorite and pyrite TiO_2. Anatase and rutile belogs to tetragonal crystal system whereas fluorite and pyrite belongs to cubic crystal system. Anatase [29], rutile [39] and fluorite [11] TiO_2 structures are created using experimental lattice parameters and wyckoff positions whereas for pyrite the lattice constants considered are $a = b = c = 4.844$ Å [25]. Structure has been optimized using maximized force of 0.005eV/Å and maximum step length of 0.5 Å. Zero constraints are considered during optimization. The Limited Memory Broyden-Fletcher-Goldfarb-Shanno (LBFGS) [47–50] is adopted for the optimization of all structures because of its effectivity for estimation of parameter in machine learning. It is based on the approximate Hessian matrix. At every iteration, it updates the approximated Hessian matrix by using products of vector–vector. With minimum iterations, it obtains its local minimum without sticking at the time of calculation. Furthermore, energy minimization is also carried out by varying lattice constants for all the structure under consideration to obtain the characteristic plotfortotal energy versus total volume, which are shown in figures 2(a) and (b) for high and normal pressure TiO_2, respectively. The lowest energy lattice constants are considered for simulation because minimizing the total energy of the crystal determines an appropriate set of linear combination of coefficients. OLCAO method [51] is applied here in the framework of Density Functional Theory (DFT), which is an all-electron technique applied for calculating $3p^6 4s^2 3d^2$ and $2s^2 2p^4$ states as valence electrons for Titanium and Oxygen atom respectively. The optimized lattice structures of fluorite, pyrite, anatase and rutileTiO_2 are shown in figures 1(a), (b), (c) and (d), respectively. The prediction of the molecular orbitals by this method is accurate due to the orthogonal simulation pattern. The LCAO method initially assumes that the

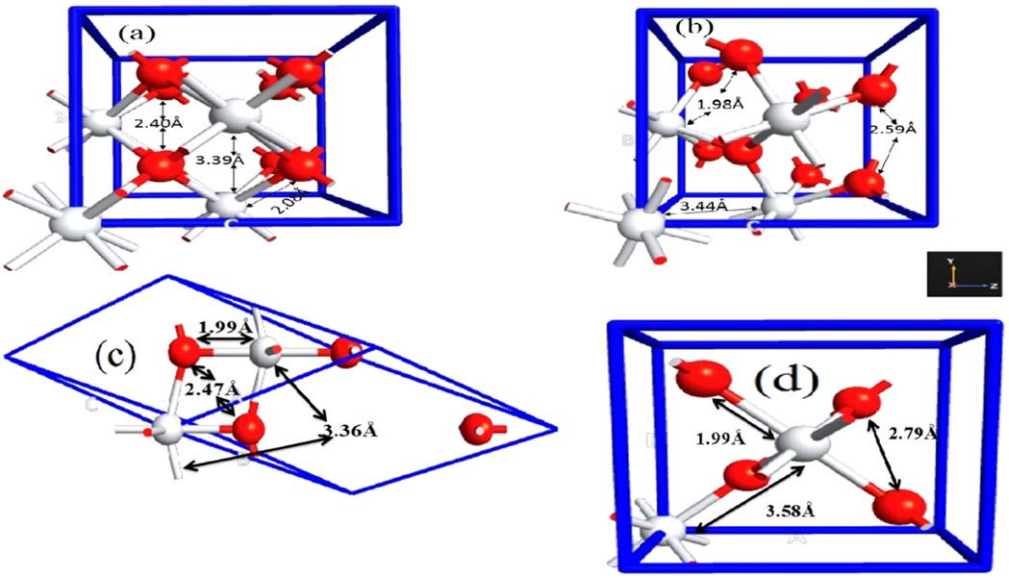

Figure 1. Optimized structures of TiO_2 (a) Fluorite (b) Pyrite (c) Anatase (d) Rutile.

total number of atomic orbitals is equal to the total number of molecular orbitals included in the linear expansion. We have used GGA with PBE SOL [52] as exchange-correlation functional. Also used MGGA-TBO_9 exchange-correlation functional to analyzed electronic and optical properties of normal pressure phases of TiO_2. Other parameters like van der Waals corrections, spin–orbit coupling and Hubbard Uare disabled. The Density mesh cut off is taken as 140 Hartree for all the structures. Sampling is done using the Monkhorst –Pack scheme [53] and set at $6 \times 6 \times 7$ for anatase and rutile, $12 \times 12 \times 12$ for fluorite and $7 \times 7 \times 7$ for pyrite. State of art norm-conserving pseudopotentials have been used [54] for both Titanium and oxygen atoms.

The biggest benefit of approximate Linear Combinations of Atomic Orbitals (LCAO) method is its correctness in observable properties of molecules over other methods. The approximations used in LCAO method are superior than that of self-consistency field calculations. In addition, the approximation used in LCAO method is benificial because they provide a relation between an orbital description and chemical intuition. GGA-PBE is most widely used approximation. PBE is the improved to PBESOL by making changes in two parameters. PBESOL provides improvement in equilibrium properties of bulk. By restoring gradient expansion for exchange, PBESOL provide lattice parameters lower than PBE and cohesive energies with less accuracy. Electronic properties such as bandgap value using GGA are underestimated because a single exchange-correlation potential is not continuous across the gap. To enhance electronic properties MGGA family of functional extend the GGA approximation by additionally depending on the Laplacian of the density and kinetic energy density. Hence, MGGA gained substantial achievement in the improvement of electronic properties.

3. Results and discussion

3.1. Structural parameter

Structural optimization of anatase, rutile, fluorite and pyrite TiO_2 is carried out by varying lattice constant and finding out the lowest energy point. For simulation, a totally relaxed Wyckoff position and experimental cell volume [11, 29, 39] is considered. The lattice constant as obtained from the figures 2(a) and (b) are $a = 4.804$ Å for fluorite and $a = 4.869$ Å for pyriteand $a = 3.796$ Å, $c = 9.617$ Å for anatase and $a = 4.616$ Å, $c = 2.961$ Å, for rutile. Table 1 represents a comparison of the calculated density, structural parameters, volume and bandgap (Eg) with previously reported theoretical and experimental values.

3.2. Electronic properties

The energy band structure is an important property of any material which describes the optical and electronic properties. The energy bandgap is defined as the minimum energy required to create an electron and hole pair in the semiconductor. Whereas, the optical bandgap is the excitation energy which determines the onset of vertical interband transitions. Two properties namely, the band structure and total density of states are studied here and analyzed in detail. Figure 3(a) represents the band structure and 3 (b) represents the total density of states (TDOS) for fluorite TiO_2. From the band diagram of fluorite TiO_2, it can be observed that Fermi energy is more

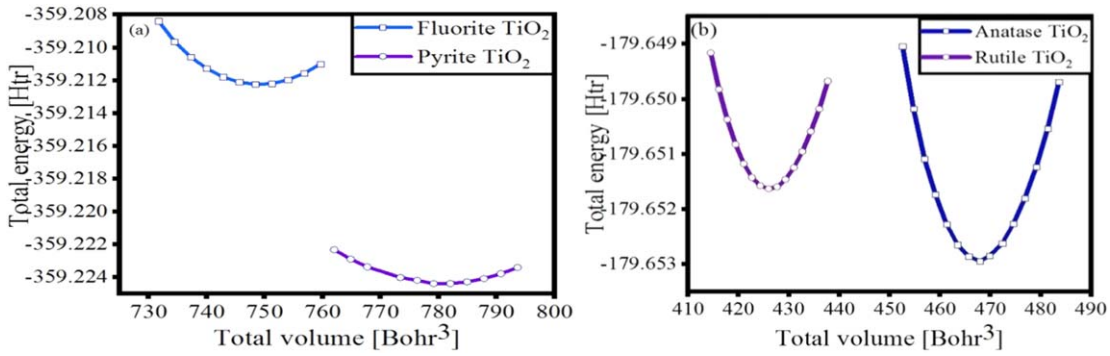

Figure 2. Total Energy versus volume of (a) High pressure phases of TiO_2 and (b) Normal pressure phases of TiO_2.

Table 1. Density, the lattice constant, volume, and bandgap of fluorite and pyrite TiO_2 in comparison with previous data where D represents direct bandgap nature and ID represents indirect bandgap nature.

Phase	Method	Density(ρ)(gm cm^{-3})	a(Å)	c(Å)	V((Å)^3)	Bandgap (eV)	References
Fluorite	OLCAO-GGA PBESOL	4.78	4.804	—	110.889	1.07(D)	This Work
	GGA-PW91	—	4.828	—	112.5	1.136(D)	[23]
	GGA-WC	—	4.786	—	110	1.123(D)	[23]
	GGA-PBESOL	—	4.782	—	109	1.120(D)	[23]
	GGA-RPBE	—	4.865	—	115	1.151(D)	[23]
	GGA	—	4.8293	—	—	1.134(ID)	[6]
	OLCAO-PZ	—	4.787	—	109.696	0.89(D)	[25]
	GGA-PW91	4.749	4.817	—	111.77	—	[31]
	Experimental	4.59	4.87	—	115.50	—	[11]
Pyrite	OLCAO-GGA PBESOL	4.59	4.869	—	115.43	1.369(ID)	This work
	GGA-PW91	—	4.891	—	117	1.466(ID)	[23]
	GGA-WC	—	4.851	—	114.2	1.472(ID)	[23]
	GGA-PBESOL	—	4.849	—	114	1.474(ID)	[23]
	GGA-RPBE	—	4.927	—	119.6	1.457(ID)	[23]
	GGA	—	4.8940	—	—	1.457(ID)	[6]
	OLCAO-PZ	—	4.844	—	113.661	1.18(ID)	[25]
	GGA-PW91	4.563	4.881	—	116.28	—	[31]
Anatase	OLCAO-GGA PBESOL	3.825	3.79685	9.61702	69.3198	2(ID)	This work
	MGGA-TBO9	—	—	—	—	3.3(ID)	This work
	GGA-PW91	—	3.784	9.712	69.539	—	[31]
	GGA-PBESOL	3.902	3.7767	9.5349	—	—	[35]
	DFT	—	3.8	9.7	—	2.13(ID)	[33]
	PBE-GGA	—	3.811	9.631	69.947	2.14(D)	[36]
	WC-GGA	—	3.784	9.512	68.066	—	[36]
	OLCAO-PZ	—	3.7842	9.5146	—	—	[29]
	EXP	—	3.785	9.512	—	—	[39],[30]
Rutile	OLCAO-GGA PBESOL	4.201	4.6164	2.9611	—	1.81	This work
	MGGA-TBO9	—	—	—	—	2.98	This work
	GGA-PW91	4.184	4.630	2.957	63.41	—	[31]
	GGA-PBESOL	4.27	4.5949	2.9433	62.1422	—	[35]
	DFT	—	4.643	2.965	63.918	1.86(D)	[33]
	PBE-GGA	—	4.634	2.976	63.912	1.94(D)	[36]
	WC-GGA	—	4.643	2.881	62.107	—	[36]
	EXP		4.593	2.959	62.420	3.0	[39], [30]

closed to the conduction band whereas, the minima energy pointof the conduction band and maxima energy point of valence band lie on the same line G, implying a direct bandgap having a value of 1.07 eV. It is seen that 14 bands are having a width equal to 7.34 eV below the Fermi level. These bands are the result of the mixing of atomic orbitals O 2p and Ti 3d. 10 bands are having a width 4.38 eV above the Fermi level. These bands are the effect ofthe Ti 3d orbitals contribution. It is observed from figure 3(b) that the highest points (peak) occur on the top of the valence and bottom of the conduction band at −2.79 eV, −1.81 eV and 2.12 eV, 2.36 eV due to mixing of atomic orbitals Ti 3d and O 2p respectively. Occupied states between oxygen 2p and titanium3d which ranges

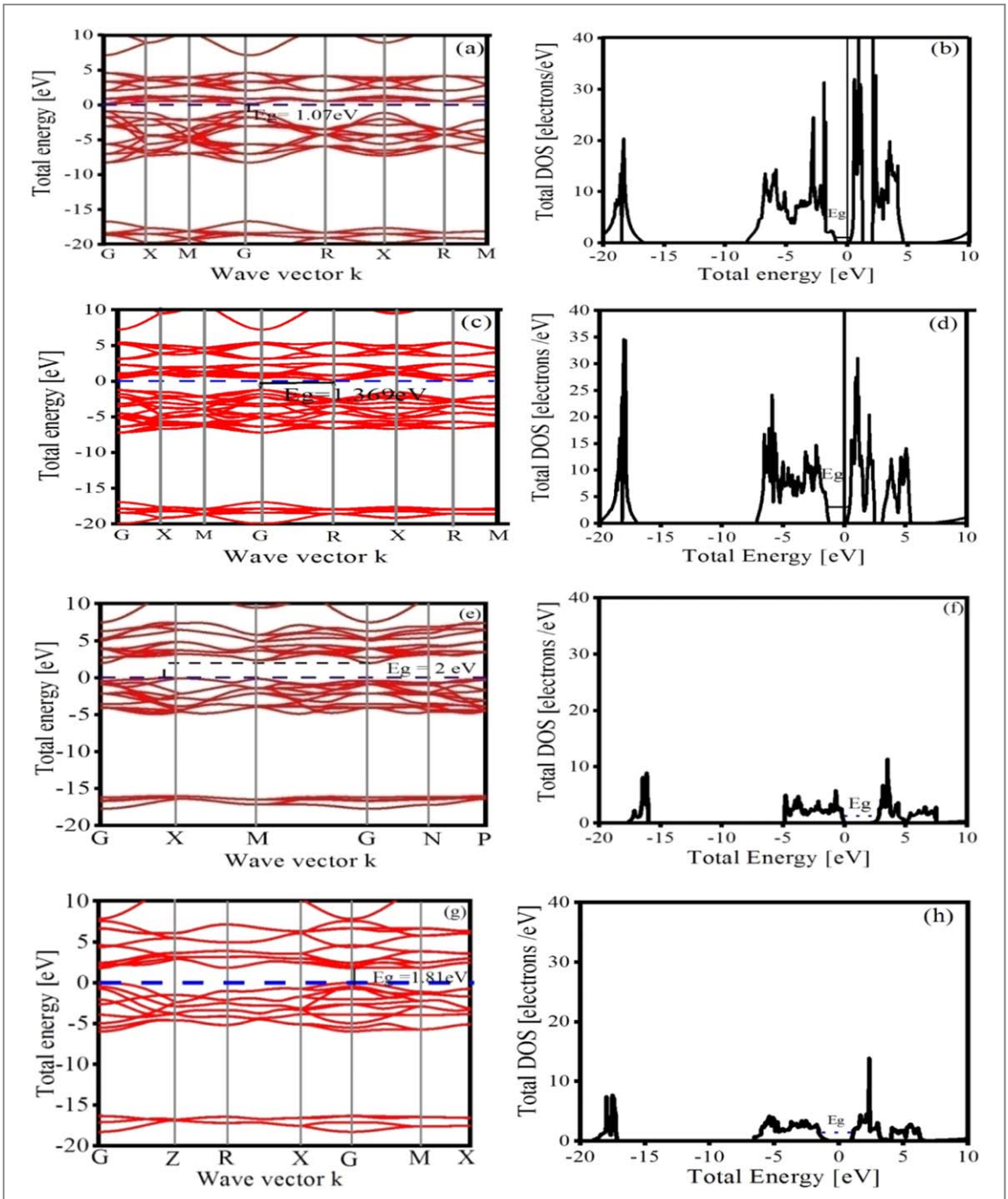

Figure 3. Bandstructure:- (a) Fluorite (c) Pyrite (e) Anatase (g) Rutile. TDOS:- (b) Fluorite (d) Pyrite (f) Anatase (h) Rutile.

from 0 to −8.269 eV are also because of the mixing of atomic orbitals and this results in more covalent bonding between Ti and O in fluorite TiO_2. Engaged energy states are from −20 to −16.66 eV, −8.22 to −0.882 eV and 0.190 eV to 1.26 eV, 2.07 to 4.63 eV in the range of energyfrom −20 eV to 10 eV. In the conduction band, the highest peaks occur due to Ti 3d contributions. Lowest of the valence bands start well before -20ev and it is the result of O 2s state contribution. Highest occupied valence band for fluorite TiO_2 is the result of atomic mixing of oxygen 1s and titanium 2p states.1s of titanium also contribute to the formation of the highest valence band, but its contribution is very less compared to Ti 2p and O 1s states. In the valence band, the highest peaks are the results of the atomic mixing of Op and O s state.Ti 2p, Ti 3d and O 2p contributed a little in the formation of the valence band.

From the band diagram of pyrite TiO_2, it can be observed that Fermi energy is more close to the conduction band. Valence band Maxima and conduction band minima lie at different points G and R in the energy band

implying pyrite TiO_2 to be of indirect bandgap having a value of 1.369 eV. Figure 3(c) represents the band structure while figure 3(d) represents TDOS of pyrite TiO_2.17 bands are having a width equal to 6.044 eV below the Fermi level. These bands are as a result of the mixing of atomic orbitals O 2p and Ti 3d. Again 10 bands are having a width of 5.034 eV above the Fermi level. These bands result from the contribution of Titanium 3d shell and Oxygen 2s shell. It is observed from figure 3(d) highest (peak) points occur on the top of valence and bottom of conduction band at −5.91 eV, −3.15 eV, −2.3 eV and 1.10 eV, 2.03 eV, 5.08 eV due to mixing of atomic orbitals Ti_3d and O 2p respectively. Occupied states between O 2p and Ti 3d ranging from 0 to −7.175 eV are also because of the mixing of atomic orbitals which indicates a more covalent bonding between Ti and O in pyrite TiO_2. The associated energy states are from −20.28 to −16.66 eV, −7.216 to −1.251 eV and 0.118 eV to 2.48 eV, 3.05 to 5.41 eV in the range of energy from −20 eV to 10 eV. In the conduction band, the highest peaks occur because of Ti-3d contributions and a very less contribution from O 2p. Lowest of valence band starts from −20 eV and it is the result of O 2s state contribution. The highest occupied valence band for pyrite is the result of the atomic mixing of oxygen 1s and titanium 2p states. Titanium 1s also contribute to the formation of the highest valence band, but its contribution is very less compared to Ti 2p and O1s states. In the valence band, major peaks are the results of the atomic mixing of O 2p and O 2s state. A small contribution of Ti 2p, Ti 3d and O 2p are there in the formation of the valence band. From the density of states, it is clear that the width of the conduction band and valence band in pyrite is smaller than fluorite, which supports a larger bandgap value of pyrite as compared to fluorite. This can be verified also from computed results.

From the band diagram of anatase TiO_2, it can be observed that Fermi energy is more close to the valence band. Valence band maxima and conduction band minima lie at different points X and G in the energy band implying anatase TiO_2 to be of indirect bandgap having a value of 2 eV. Bandgap value obtained using MGGA-TBO9 is 3.3 eV which is 3% higher than experimental value [30]. Figure 3(e) represents the band structure while figure 3(f) represents the TDOS of anatase TiO_2. Bands below the Fermi level are having a width equal to 4.13 eV. These bands are as a result of the mixing of atomic orbitals O 2p and Ti 3d. Bands above the Fermi level are having a width of 5.46 eV. These bands result from the contribution of Titanium 3d shell and Oxygen 2s shell. It is observed from figure 3(f) highest (peak) points occur on the top of valence and bottom of conduction band at −16.22 eV, −5.082 eV and 3.04 eV, 11.43 eV due to mixing of atomic orbitals Ti 3d and O 2p respectively. In the valence band, major peaks are the results of the atomic mixing of O 2p and O 2s state. A small contribution of Ti 2p, Ti 3d and O 2p are there in the formation of the valence band.

Figure 3(g) represents the band structure and 3 (h) represents the TDOS for rutile TiO_2. From the band diagram of rutile TiO_2, it can be observed that Fermi energy is more close to the valence band whereas the minima energy point of the conduction band and maxima energy point of valence band lie on the same line G, implying a direct bandgap having a value of 1.81 eV. Bandgap value obtained using MGGA-TBO9 is 2.98 eV which is 0.6% lower than experimental value [30]. Bands below the Fermi level are having a width equal to 5.95 eV. These bands are as a result of the mixing of atomic orbitals O 2p and Ti 3d. Bands above the Fermi level are having a width of 6 eV. These bands result from the contribution of Titanium 3d shell and Oxygen 2s shell. It is observed from figure 3(f) highest (peak) points occur on the top of valence and bottom of conduction band at −17.45 eV and 2.435 eV due to mixing of atomic orbitals Ti 3d and O 2p respectively. In the valence band, major peaks are the results of the atomic mixing of O 2p and O 2s state. A small contribution of Ti 2p, Ti 3d and O 2p are there in the formation of the valence band.

3.3. Effective mass of electron and hole (m^*)

It is the mass of charge carriers (e−/h+) when they respond to any type of interaction in a crystal lattice. The effective mass highly depends on the crystal structure or electronic band structure in solids [33]. It is usually stated in the unit of the rest mass of an electron, m_e (9.11×10^{-31} kg). Equation (1) represents, the transfer rate of photogenerated electrons and holes which is inversely proportional to effective mass.

$$v = \frac{\hbar k}{m^*} \tag{1}$$

Where, m^* representsan effective mass of (e−/h+), k is the wave vector,ħ is Planck constant, v is the transfer rate of photogenerated electrons and holes. Thus, a smaller effective mass is desired to get higher photocatalytic activity. Effective mass isusually calculated using equation (2) and is represented as

$$m^* = \hbar^2 \left(\frac{d^2E}{dk^2} \right)^{-1} \tag{2}$$

Where, E is the energy of an electron at wavevector k in that band. Table 2 gives a comparison of the calculated effective mass of cubic TiO_2 with an effective mass of other phases of TiO_2. From table 2, m^* of an electron in pyrite is smaller than fluorite and brookite but it is higher than anatase and rutile. The transfer rate of hole and electrons in pyrite is faster than fluorite. This leads to higher photocatalytic activity in pyrite than fluorite. Also,

Table 2. Comparison of the calculated effective mass of cubic TiO_2 with an effective mass of other phases of TiO_2.

Phase	The effective mass of the electron (m^*)	The effective mass of hole (m^*)
Fluorite [This work]	0.514(average of m^* from Γ to R and Γ to M)	0.1205 (average of m^* from Γto R and Γ to M)
Pyrite [This work]	0.3195 (average of m^* from Γto R and Γ to M)	0.4225 (average of m^* from Γto R and Γ to M)
Anatase [33]	0.0948(average of m^* from G to Z and G to M)	0.1995(average of m^* from B to G and B to M)
Rutile [33]	0.0949(average of m^* from G to Z and G to M)	0.5620(average of m^* from G to Z and G to M)
Brookite [33]	1.4610(m^* from G to Z)	0.4345(m^* from G to Z)

pyrite is an indirect bandgap semiconductor, therefore conduction band minima aad valence band maxima lies at different k points. Thus, a lifetime of photogenerated electron and hole increases in pyrite compared to fluorite. This is in agreement with [33], that indirect bandgap semiconductor has better photocatalytic activity than direct bandgap semiconductor.

3.4. Optical properties

The optical properties are calculated by considering energy level up to the phonon energy, (40 eV), for cubic phases and (12 eV) for tetragonal phases using GGA-PBE SOL. MGGA-TB09 is used to calculate optical properties of normal pressure phases of TiO_2. For calculating the optical properties, equations given in ref [33] are used. As the dielectric function is a complex quantity and so it contains real and imaginary parts. The real part gives an idea about the electronic polarizability of material and the imaginary part gives an idea about the absorption of the material. For evaluating dielectric function Kubo-Greenwood formalism [55, 56] has been implemented. From figures 4(a), (b) and figures 5(a), (b) the value of the $\varepsilon_1(0)$ for fluorite, pyrite, anatase and rutile TiO_2 are found to be 8.82, 8.17, 6.9 and 8 respectively using GGA-PBES. The value of $\varepsilon_1(\omega)$ for normal pressure phases are in good agreement with experimental data [57, 58]. Using MGGA-TB09, $\varepsilon_1(0)$ for anatase and rutile TiO_2 is found to be 5.794 and 5.913 which are very close to experimental value [40, 59]. The highest peak of $\varepsilon_1(\omega)$ occurs at 3.13 eV for fluorite, 2.27 eV for pyrite, 3,14 eV for anatase and 2.68 eV for rutile. These peaks are the effect of titanium 3d and oxygen 2p states contributions. The refractive index gives an idea about the optical density of the medium. If its value is large thenit implies that speed of light is less i.e. density is more. The refractive indices of anatase, rutile, fluorite and pyrite are 2.627, 2.828, 2.98 and 2.85 respectively. Refractive index of anatase and rutile using MGGA-TB09 are 2.407 and 2.469 respectively, which are close to experimental data [41, 42]. From the observed data, we can say that dielectric function is equal to the square of the refractive index. The refractive index is a complex quantity and the extinction coefficient k (ω) represents its imaginary part.It gives an idea about light absorption. Figures 4(c),(d) and figures 5(c),(d) shows the plot of $\eta(\omega)$ for high pressure and normal pressure phases TiO_2 whereas figure 4(e), (f) and figure 5(e), (f) shows the plot of k(ω) for anatase, rutile, fluorite and pyrite TiO_2 respectively. From figures 4(g), (h) and figures 5(g), (h) a sharp decline in reflection spectra can be observed at 9.37 eV for anatase, 7.70 eV for rutile, 14.017 eV for fluorite and 13.096 eV for pyrite. Again, from the figures 4(g), (h) and (g), (h) it is evident that fluorite, pyrite, anatase and rutile reflect around 24.5%, 23.4%, 20.1% and 22.8% of the incident light radiation. Using MGGA-TB09 value of R(0) is 0.17 and 0.179 respectively. The L(ω) is the loss of energy of electrons when they pass through a uniform dielectric material. Here the energy peaks of L(ω) occur at 14 eV for fluorite and 13 eV for pyrite. Energy peaks of the loss function and a sharp decline in reflection spectra are matching towards each other for all the structure which is represented by figures 4(m), (n) and figures 5(m), (n) for fluorite , pyrite, anatase and rutile TiO_2 respectively. Figures 4(i) and (j) represent absorption spectra Versus energy for fluorite and pyrite TiO_2 respectively. Figures 5 (i) and (j) represent absorption spectra Versus energy for anatase and rutile TiO_2 respectively. Figures 4(k), (l) and figures 5(k), 4(l) represent absorption spectra Versus wavelength for fluorite, pyrite, anatase, and rutile respectively. It gives an idea about the penetration of the light of a particular λ into the material before it is absorbed. The fluorite is having a more absorptive transition in the visible region than the pyrite. Major peaks of the R(ω) occur in the same energy limit as $\alpha(\omega)$ for all the structures. In the case of fluorite, major peaks occur within the energy range of 0 to 15 eV for both reflection and absorption spectra whereas, it occurs within the energy range of 0 to 14 eV for pyrite TiO_2. As high pressure and normal pressure phases of TiO_2 are behaving as direct and indirect bandgap semiconductor, when the bombardment of a photon with energy greater than bandgap energy takes place, it results in the creation of electron-hole pairs and this phenomenon is known as photoconductivity. This process is important for solar cell application as it involves the conversion of non-electrical energy into electrical energy. Photoconductivity is directly proportional to dielectric function. This relationship is very much apparent from figure 4(a)–(b) , figures 5(a)–(b) and figures 4(o)–(p), figures 5(o)–(p). Figures 4(o), (p) and figures 5(o), (p) represent photoconductivity for fluorite, pyrite, anatase and rutile TiO_2 respectively. The absorption of phonon is directly proportional to electrical conductivity. Both fluorite and pyrite have very

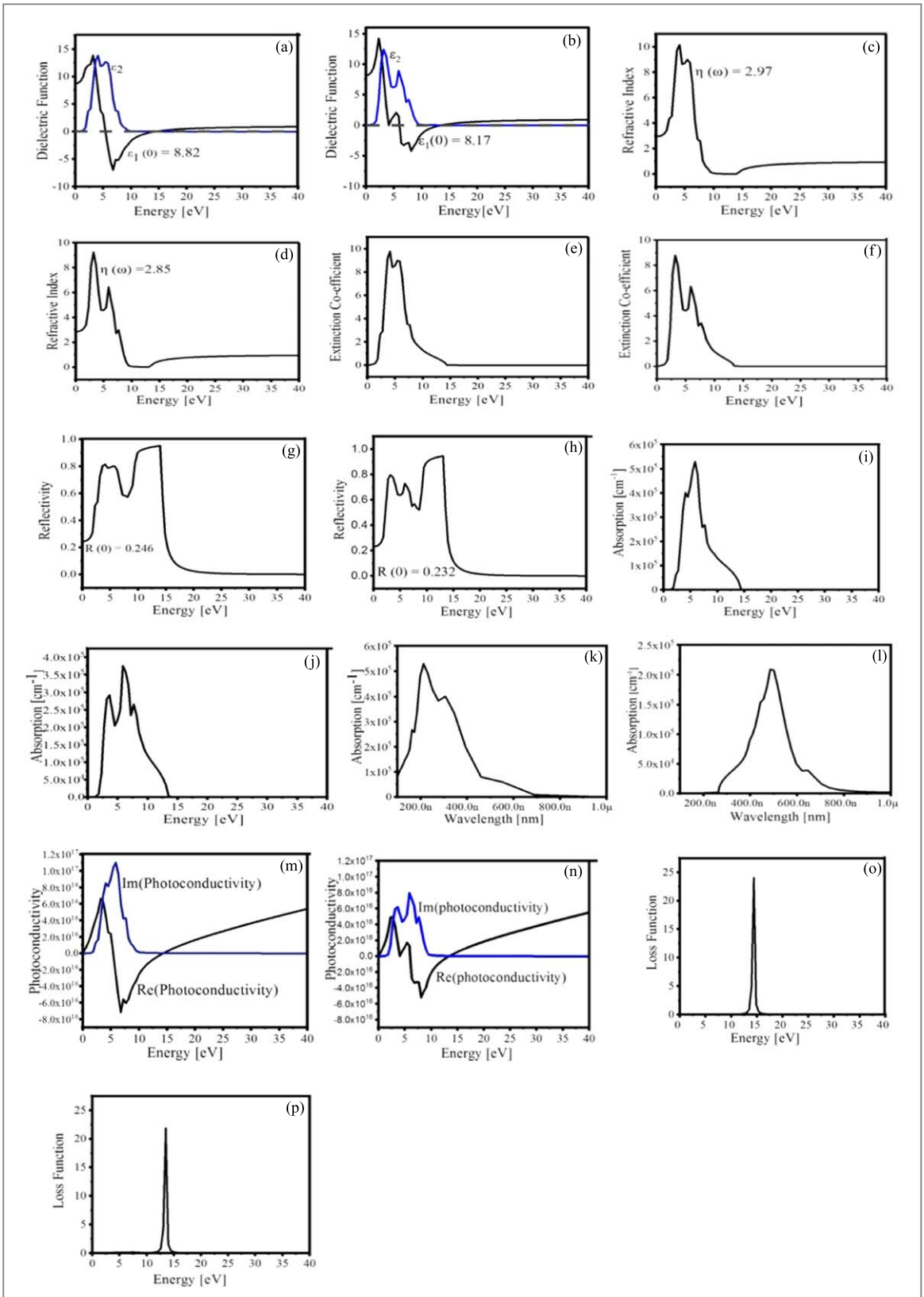

Figure 4. fluoriteTiO_2:-. (a)$\varepsilon_1(\omega)$, (c)$\eta(\omega)$, (e)k(ω), (g)R(ω), (i)$\alpha(\omega)$, (k)$\alpha(\omega)$Versus wavelength, (m)photoconductivity, (o)L(ω) Pyrite TiO_2:-(b) $\varepsilon 1(\omega)$, (d) $\eta(\omega)$, (f)k(ω), (h)R(ω), (j)$\alpha(\omega)$, (l)$\alpha(\omega)$Vswavelength, (n)photoconductivity, (p)L(ω)

good absorption value which ranges from 0 to 15 eV of photon energy for fluorite and 0 to 14 eV for pyrite TiO_2. Therefore, cubic TiO_2can provide good electrical conductivity. Table 3 represents the comparison of calculated $\varepsilon_1(0)$, $\eta(0)$ and R(0) with previously reported data.From reflectivity spectra, it is found that TiO_2 can provide good electrical conductivity and very much suitable as a coating material.

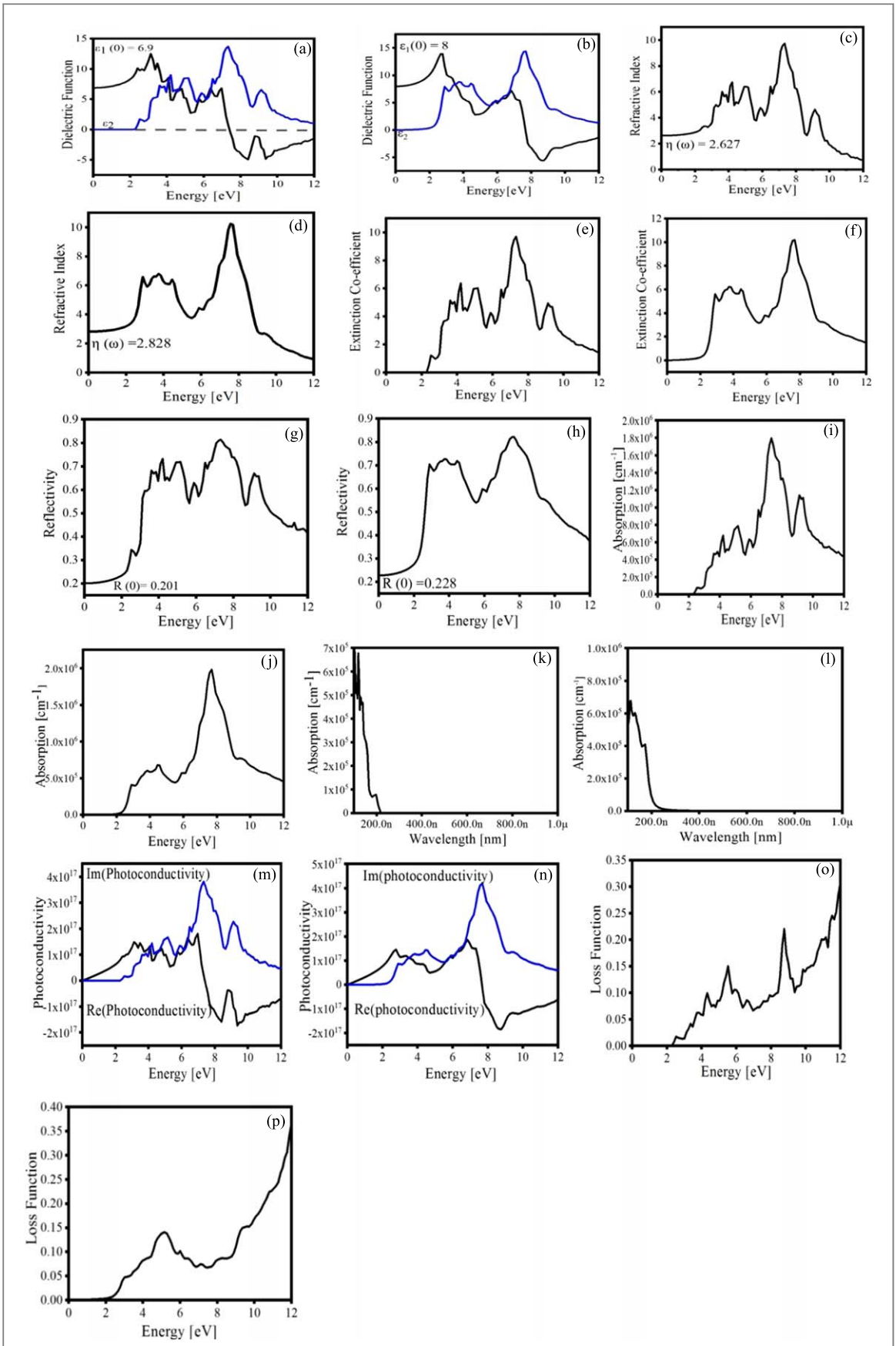

Figure 5. anatase TiO_2 :-(a) $\varepsilon 1(\omega)$, (c)$\eta(\omega)$, (e)k(ω), (g)R(ω), (i)$\alpha(\omega)$, (k)$\alpha(\omega)$Vs wavelength, (m)photoconductivity, (o)L(ω) Rutile TiO_2:- (b) $\varepsilon 1(\omega)$, (d) $\eta(\omega)$, (f) k(ω), (h) R(ω), (j) $\alpha(\omega)$, (l) $\alpha(\omega)$Vs wavelength, (n)photoconductivity, (p)L(ω).

Table 3. Comparison of calculated $\varepsilon_1(0)$, $\eta(0)$ and R(0) of fluorite , pyrite, anatase and rutile TiO_2 with previously available data.

Phase	Method	($\varepsilon_{xx}(0)$)	($\varepsilon_{zz}(0)$)	($\eta(0)$)	(R(0))	References
Fluorite	GGA-PBESOL	8.82		2.98	0.245	This work
	GGA-PBESOL	7.64		2.76	—	[23]
	GGA-RPBE	7.72		2.78	—	[23]
	GGA-WC	7.67		2.77	—	[23]
	GGA-PW91	7.70		2.77	—	[23]
	LDA-PZ-OLCAO	4.7		2.2	—	[32]
	LDA	7.348		2.711		[6]
Pyrite	GGA-PBESOL	8.17		2.85	0.234	This work
	GGA-PBESOL	7.46		2.73	—	[23]
	GGA-RPBE	7.42		2.72	—	[23]
	GGA-WC	7.46		2.73	—	[23]
	GGA-PW91	7.44		2.73	—	[23]
	LDA-PZ-OLCAO	3.75		1.90	—	[32]
	LDA	7.345		2.710	—	[6]
Anatase	GGA-PBESOL	6.87	6.96	2.627	0.201	This work
	MGGA-TB09	5.828	5.727	2.407	0.170	This work
	GGA	6.75	6.44	—	—	[26]
	mBJ	5.35	5.21	—	—	[26]
	BSE	5.12	4.98	—	—	[37]
	GGA + U^d + U^p	6.137	5.995	2.315	—	[38]
	Exp	—	—	2.3	—	[41]
	Exp	5.8	5.4	—	—	[59]
	Exp	6.55	6.20			[57]
Rutile	GGA-PBESOL	7.53	8.94	2.828	0.228	This work
	MGGA-TB09	5.716	6.864	2.469	0.179	This work
	GGA	7.34	8.68	2.79	—	[26]
	mBJ	5.75	6.70	2.46	—	[26]
	BSE	5.71	7.33		—	[37]
	GGA + U^d + U^p	6.298	5.485	2.605	—	[38]
	Exp	—	—	2.6	—	[42]
	Exp	—	—	2.55	—	[60]
	Exp	5.7	7.0	—	—	[40]
	Exp	6.84	8.43	—	—	[58]

3.5. Mechanical properties

Mechanical properties give an idea about the nature of forces acting in solids, phonon spectra, and interatomic potential and thereby specifying its hardness, stability, etc. Before doing all the calculations we checked positive definiteness of stiffness matrix [43, 61] using equation (3) for cubic phase,

$$c_{11} > |c_{12}|.c_{11} > 0,\ c_{44} > 0,\ (c_{11} + 2c_{12}) > 0 \tag{3}$$

Tetragonal phase will be mechanically stable, if it satisfies the Born–Huang criteria [62]

$$(c_{11} - c_{12}) > 0,\ (c_{11} + c_{33} - 2c_{13}) > 0,\ 2(c_{11} + c_{12})c_{33} + 4c_{13}) > 0,\ c_{11},\ c_{33},c_{44},\ c_{66} > 0 \tag{4}$$

If equation (3) is fulfilled by cubic material then it is considered as mechanically stable and if equation (4) is fulfilled by tetragonal material then it is considered as mechanically stable. Table 4 gives a comparison of calculated elastic properties with previously reported data. Elastic compliance s_{ij} are calculated using equations given in [63]. Table 5 shows the comparision of Elastic compliance sij for fluorite, pyrite, anatse and rutile TiO_2 with available theoretical data. From table 4, it is apperant that cubic and tetragonal phase TiO_2 satisfies respective equations (3) and (4) and hance they are mechanically stable.

Again, Bulk and shear moduli are used to measure the hardness of the material. Two different theories are there to calculate the bulk and shear modulus namely, Reuss theory [67] and Voigt theory [68]. According to Reuss Theory B_R and G_R are given by

$$B_R = (3s_{11} + 6s_{12})^{-1} \text{and } G_R = 5(4s_{11} - 4s_{12} + 3s_{44})^{-1} \tag{5}$$

Where, s_{11}, $s_{12,}$and s_{44} are the compliance matrix elements of cubic TiO_2. According to Voigt Theory B_V, G_V is given by

Table 4. Elastic constant c_{ij} for fluorite, pyrite, anatse ans rutile TiO_2.

Phase	Method	C_{11}	C_{12}	C_{13}	C_{33}	C_{44}	C_{66}	References
Fluorite	OLCAO-PBES	631.63	88.53	—	—	25.08		[This work]
	GGA-PBES	634	87.5	—	—	36		[23]
	GGA-PW91	603	75	—	—	43		[32]
	OLCAO-PZ	523.09	180.66	—	—	32.6		[25]
	GGA	599.7	73.8	—	—	29.6		[6]
Pyrite	OLCAO-PBES	431.84	170.71	—	—	95.97		[This work]
	GGA-PBES	427	177	—	—	93.26		[23]
	GGA-PW91	413	159	—	—	96		[31]
	OLCAO-PZ	430.58	190.70	—	—	88.39		[25]
	GGA	405.8	160.1	—	—	93.1		[6]
Anatase	OLCAO-PBES	264.13	189.66	164.225	482.88	118.25	231.86	[This work]
	PBESOL	355.86	155.05	147.74	207.41	74.41	60.62	[35]
	GGA	338	136	147	193	51	60	[31]
	GGA	323.4	147.4	140.9	198	51.7	59.3	[34]
	OLCAO-PZ	379	135	184	180	37	47	[29]
Rutile	OLCAO-PBES	264.13	189.66	164.225	482.88	118.25	231.86	This work
	PBESOL	297.79	168.89	158.51	498.32	122.71	229	[35]
	GGA	267	165	152	483	122	212	[31]
	GGA	258	163.2	146.1	468.1	115.4	211.3	[34]
	PBESOL	276	200	163	497	118	230	[27]
	EXP(298K)	271	177	149	484	124	194	[64]
	EXP(300K)	267	174	146	484	124	190	[65]
	EXP(4K)	289	197	159	508	128	227	[66]

Table 5. Elastic compliance matrix non zero values (s_{ij}) for fluorite, pyrite, anatase and rutile TiO_2.

Phase	Method	S_{11}	S_{12}	S_{13}	S_{33}	S_{44}	S_{66}
Fluorite	OLCAO-PBES [This work]	0.00164	−0.0002	—	—	0.03987	—
Pyrite	OLCAO-PBES [This work]	0.00298	−0.00085	—	—	0.01042	—
Anatase	OLCAO-PBES [This work]	0.004415	−0.00051	0.003212	0.010915	0.026483	0.018002
	PBESOL [35]	0.0041542	−0.0008256	−0.0023711	0.0081996	0.0133782	0.0164957
Rutile	OLCAOPBES [This work]	0.008175	−0.00525	0.000994	0.002747	0.008457	0.004313
	PBESOL [35]	0.0052447	−0.0025111	−0.0008695	0.0025599	0.081493	0.0043668

$$B_V = \frac{(c_{11} + 2c_{12})}{3},\ G_V = \frac{(c_{11} - c_{12} + 3c_{44})}{5} \tag{6}$$

According to the Hill [69] approximation, the bulk modulus B_{Hill} and shear modulus G_{Hill} is given by

$$B_{Hill} = \frac{(B_R + B_V)}{2},\ G_{Hill} = \frac{(G_R + G_V)}{2} \tag{7}$$

While Vicker's hardness [70] is also used to check the hardness of the material and it is given by

$$H_V = 2(k^2G)^{0.585} - 3 \tag{8}$$

Obtained Vicker's hardness show that rutile is harder than other three polymorphs of TiO_2 where, k = G/B = Pugh's modulus ratio. Young's modulus is the measure of the stiffness of the material and it is given by

$$E = \frac{9BG}{G + 3B} \tag{9}$$

Poisons ratio (v) is used to classify material and to check the ductile and brittle property of the material. v = 0.25 [71, 72] for ionic material v = small approximately equal to 0.1 [69, 73] for covalent materials. For brittle material,v<0.33 and for ductile materialv>0.33.Poisons ratio (v) [69, 73] is given by

$$v = \frac{1}{2}\left[\frac{B - \left(\frac{2}{3}\right)G}{B + \left(\frac{1}{3}\right)G}\right] \tag{10}$$

Table 6. Mechanical properties of cubic TiO_2:- B, G, E, λ are in (GPa) and Hv,A,v, (B/G)are dimensionless parameters.

Phase	Method	B	A	G	B/G	E	v	Hv	λ
fluorite	GGA-PBES [This work]	269.19	0.092	81.5	3.30	222.14	0.3626	3.48	214.84
	GGA-PBES [23]	270	—	55	—	612	0.121	—	—
	GGA-PW91 [32]	251	—	131	—	336	0.277	—	—
	OLCAO-PZ [25]	296.2	0.19	68.1	—	431.03	0.393	1.23	—
	GGA [6]	249.1	—	84.4	—	227.5	0.348	—	—
	GGA [34]	249.1		84.4	—	227.5	0.348		192.8
	Exp [44]	202	—	—		—	—	—	—
Pyrite	GGA-PBES [This work]	259.08	0.735	108.57	2.38	285.8	0.316	8.22	—
	GGA-PBES [23]	262.11	—	103.4	—	320	0.30	—	—
	GGA-PW91 [31]	244	—	108	—	283	0.306	—	—
	OLCAO-PZ [25]	270.83	0.73	99.9	—	313.47	0.335	5.94	—
	GGA [6]	242.0	—	104.0	—	272.9	0.312	—	—
	GGA [27]	242.0		104	2.327	272.9	0.312	—	172.7
Anatase	OLCAO-PBES This work	182.7	0.547	48.65	3.75	134.07	0.377	—	134.07
	GGA-PBESOL [35]	194.19	—	71.03	2.73	189.93	—	10.47	—
	GGA-PW91 [31]	192	—	62	3.12	167	—	—	—
	GGA [34]	182.9	—	58.5	3.126	158.6	0.355	—	143.9
	GGA-PBESOL [27]	191	—	56	3.43	152	0.37	—	—
	OLCAO-PZ [29]	198.07	0.3	45	4.3	177	0.39	—	—
	EXP [2]	179	—	—	—	—	0.355	—	—
Rutile	OLCAO-PBES [This work]	222.04	6.22	99.75	2.225	260.29	0.304	11.583	260.29
	GGA-PBES [35]	224.67	—	124.87	1.80	316.06	—	—	—
	GGA-PW91 [31]	217	—	128	1.70	320	—	—	—
	GGA [34]	205.2	—	110.5	1.857	281.1	0.272	—	131.5
	GGA-PBESOL [27]	229	—	109	2.10	281	0.29	—	—
	Exp [74, 75]	212-235	—	—	—	—	—	—	—

From the calculated ν, we cay say that all the four structures are ductile in nature. If A = 1, the material is isotropic else the material is anisotropic. Anisotropy (A) of material is calculated using equation (11) for cubic phase and equation (12) for tetragonal phase

$$A = \frac{2c_{44}}{(c_{11} - c_{12})} \tag{11}$$

$$A = \frac{2c_{66}}{(c_{11} - c_{12})} \tag{12}$$

From calculated A, it is clear that all the structures are anisotropic in nature. Lame constant (μ, λ) are calculated using the following equation

$$\lambda = \frac{uE}{[(1 + \nu)(1 - 2\nu)]} \tag{13}$$

Table 6 gives a comparison of calculated mechanical properties with previously reported data.

4. Conclusion

This paper presents a comparative study on the optical, mechanical, structural and electronic properties of normal and high pressure phases of TiO_2 using OLCAO-GGA-PBE-SOL for the first time. MGGA-TBO9 reults on electronic and optical properties of normal pressure phases of TiO_2 are also analyzed. The computed results are then compared with the previously reported experimental and theoretical data. From the comparision, we can find that lattice constant for anatase and rutile vary only by 0.4% from experimental data [39] whereas it shows 1.3% variation with experimental data for fluorite [11]. However results are much better than the theoretical data [6, 25, 33, 34]. Bandgap values calculated using OLCAO-GGA-PBE-SOL for all the phases of TiO_2 are consistent with other theoretical data but underestimated compared to experimental data [30]. Bandgap values obtained using MGGA-TBO9 is the approximation of experimental data [30]. Effective mass analysis of cubic TiO_2 shows that transfer rate is faster in pyrite and hence exhibits higher photocatalytic activity than fluorite. Dielectric constant value calculated using OLCAO-GGA-PBE-SOL for all the structure are higher than other theoretical data [6, 23, 26, 32, 38]. Dielectric constant value for anatase and rutile using GGA-PBES are close to the experimental value [57, 58]. Dielectric constant and refractive index calculated using

MGGA-TBO9 for anatase and rutile are very much close to experimental data [40, 41, 59, 60] and better than [26, 37, 38]. Elastic constat of rutile TiO_2 are in excellent agreement with experimental data[65]. Obtained bulk modulus value for anatase, rutile and fluorite vary by 2%,4.7% and 33% from experimental data [2, 44, 74] and better than [27, 29, 31, 35]. As experimental data of pyrite TiO_2 is not available, obtained properties are compared withother theoretical data and results are found to be consistent with previously reported data.

OLCAO-GGA-PBE-SOL provides better results for structural and mechanical properties of normal pressure phases compared to high pressure phases. MGGA-TB09 reults on optical and electronic properties are the approximation of experimental data. This comparative analysis of TiO_2 using OLCAO-GGA-PBE-SOL and MGGA-TB09 will be helpful for future theoretical as well as experimental investigations.This analysis can be also helpful to study various properties of other material using the two methods described earlier.

5. Future scope

Among many candidates for photo-catalysts, TiO_2 is the only material suitable for industrial use because of its efficient photoactivity, the highest stability and lowest cost. Also it is suitable for solar cell applications. Both these applications required small bandgap material. But TiO_2 exibits large bandgap value. So, to make it suitable for above application one need to narrow the the bandgap using suitable metal and non-metal doping. So, one can verify the properties of doped and undoped TiO_2 using two methods mentioned in this paper. This will help to find its future applications.

ORCID iDs

Neerja Dharmale https://orcid.org/0000-0002-1624-454X
Debashish Dash https://orcid.org/0000-0002-5589-2267

References

[1] Li Q J and Liu B B 2016 *Chin. Phys. B* **25** 076107
[2] Arlt T, Bermejo M, Blanco M A, Gerward L, Jiang J Z, Staun Olsen J, Recio J M and Recio J M 2000 *Phys. Rev. B* **61** 14414
[3] Pischedda V, Hearne G R, Dawe A M and Lowther J E 2006 *Phys. Rev. Lett.* **96** 035509
[4] Park S, Jang J, Cheon J, Lee H H, Lee D R and Lee Y 2008 *J. Phys.Chem. C* **112** 9627
[5] Zhu T and Gao S-P 2014 *J. Phys. Chem. C* **118** 11385
[6] Li Q J, Cheng B Y, Tian B L, Liu R, Liu B, Wang F, Chen Z Q, Zou B, Cui T and Liu B B 2014 *RSC Adv.* **4** 12873
[7] Li Q J, Cheng B Y, Yang X, Liu R, Liu B, Liu J, Chen Z Q, Zou B, Cui T and Liu B B 2013 *J. Phys. Chem. C* **117** 8516
[8] Dong Z H and Song Y 2015 *Can. J. Chem.* **93** 165
[9] Yang H G, Sun C H, Qiao S Z, Zou J, Liu G, Smith S C, Cheng H M and Lu G Q 2008 *Nature* **453** 638
[10] Etgar L, Zhang W, Gabriel S, Hickey S G, Nazeeruddin M K, Eychmuller A, Liu B and Gratzel M 2012 *Adv. Mater.* **24** 2202
[11] Asahi R, Morikawa T, Ohwaki T, Aoki K and Taga Y 2001 *Science* **293** 293269
[12] Chen X and Mao S S 2007 *Chem. Rev.* **107** 2891
[13] Chen X B, Liu L and Huang F Q 2015 *Chem. Rev.* **44** 1861
[14] Samat M H, Adnan N, Taib M F M, Hassan O H, AYahya M Z and Ali A M M 2016 *Solid State Science and Technology.* **24** 2107–20
[15] Lagarec K and Desgreniers S 1995 *Solid State Commun.* **94** 519
[16] Gerward L and Staun Olsen J 1997 *J. Appl. Cryst.* **30** 259
[17] Dubrovinsky L S, Dubrovinskaia N A, Swamy V, Muscat J, Harrison N M, Ahuja R, Holm B and Johansson B 2001 *Nature* **410** 653–4
[18] Swamy V and Muddle B C 2007 *Phys. Rev. Lett.* **98** 035502
[19] Gao X, Kong C-P, Jia R, Jian W, Wang J, Bai F-Q and Zhang H-X 2018 *Solar Energy* **176** 545–55
[20] Hao L, Wang J, Bai F-Q, Xie M and Zhang H-X 2015 *Eur. J. Inorg. Chem.* **33** 5563–70
[21] Azevedoa D H M, Fabrisb G S L, Sambranob J R and Cordeiro J M M 2020 *Computational Materials Science* **171** 109222
[22] Luis W L, Rego G C, Bai F-Q, Kong C-P and Zhang H-X 2014 *RSC Adv.* **4** 19690
[23] Mahmood T, Cao C, Tahir M, Idrees F, Ahmed M, Tanveer M, Aslam I, Usman Z, Ali Z and Hussain S 2013 *Physica B* **420** 74
[24] Liang Y, Zhang B and Zhao J 2008 *Phys. Rev. B* **77** 1
[25] Dash Debashish, Pandey C K, Chaudhury S and Susanta K T 2018 *Chin. Phys. B* **27** 017102
[26] Gong S and Liu B-G 2012 *Chin. Phys. B* **21** 057104
[27] Mei Z-G, Shang Y W and Liu Z-K 2014 *Computational Material Science* **83** 114–9
[28] Sharma S, Sharma J and Sharma Y 2016 *American Institute of Physics conf proc* **1728** 020095
[29] Dash Debashish, Pandey C K, Chaudhury S and Susanta K T 2018 *MMMS* **27** 017102
[30] Reyes-Coronado D, Rodriguez-Gattorno G, Espinosa-Pesquira M E, Cab C, Coss R d and Oskam G 2008 *Nanotechnology* **19** 145605
[31] Ma X G, Liang P, Miao L, Bie S W, Zhang C K, Xu L and Jiang J J 2009 *Physics. Status Solid B* **246** 2132–9
[32] Dash D, Chaudhury C K P S and Tripathy S K 2018 *Advances in Science and Technology Research Journal* **12** 223–32
[33] Zhang J, Zhou P, Liu J and Yu J 2014 *Phys. Chem.Chem.Phys.* **16** 20381–6
[34] Li Q J, Ning-Chao Z, Fu-Sheng L and Zheng-Tang L 2014 *Physica scripta* **89** 075703
[35] Ding Y and Xiao B 2014 *Computational Material Science* **82** 202–18
[36] Mohamad M, Haq B U I, Ahmed R, Shaari A, Ali N and Hussain R 2015 *Materials Science in Semiconductor Processing* **31** 405–14
[37] Zhu T and Gao S-P 2014 *The Journal of Physical Chemistry C* **118** 11385–96
[38] Jinping L, Songhe M, Liyuan Q and Lu H 2017 *2016Chin. Phys. B* **26** 087101

[39] Burdett J K, Hughbanks T, Miller G J, Richardson J W and Smith J V 1987 *Chem Soc* **109** 3639
[40] Cardona M and Harbeke G 1965 *Phys. Rev* **137** A1467
[41] Jellison G E, Boatner L A, Budai J D, Jeong B S and Norton D P 2003 *J. Appl. Phys.* **93** 9537
[42] Schubert M, Rheinlander B, Woollam J A, Johs B and Herzinger C M 1996 *J. Opt. Soc. Am. A* **13** 875
[43] Born M and Huang K 1982 *Dynamical Theory and Experiment Springer* **1**
[44] Mattesini M, Almeida J S, de, Dubrovinsky L, Dubrovinskaia N, Johansson B and Ahuja R 2004 *Phys. Rev. B* **70** 212101
[45] Landmann M, Rauls E and Schmidt W G 2012 *J. Phys.: Condens. Matter* **24** 1
[46] Tran F and Blaha P 2009 *Physical Review Letters* **102** 226401
[47] Broyden C G 1970 *J. Inst. Maths Applics* **6** 76
[48] Fletcher R 1970 *Computer Journal* **13** 317
[49] Goldfarb D 1970 *Mathematics of Computation* **24** 23
[50] Shanno D F 1970 *Mathematics of Computation* **24** 657
[51] Ching W Y, Xu Y N and French R H 1996 *Phys. Rev. B* **54** 13546
[52] Perdew *et al* 2008 *Phys. Rev. Lett.* **100** 136406
[53] Monkhorst H J and Pack J D 1976 *Phys. Rev. B* **13** 5188
[54] Schlipf M and Gygi F 2015 *Computer Physics Communications* **196** 36–44
[55] Ching W Y and Yong-Nian Xu R H F 1996 *Phys. Rev. B* **54** 1913546–13550
[56] Desjarlais M P 2005 *Contrib. Plasma Phys.* **45** 300–4
[57] Lee C, Ghosez P and Gonzw X 1994 *Phys. Rev. B.* **50** 13379
[58] Montanari B and Harrison N M 2002 *Chem. Phys. Lett.* **364** 528
[59] Hosaka N, Sekiya T, Satoko C and Kurita S 1997 *J.Phys.Soc.Jpn* **66** 877
[60] Cardona M and Gunther H 1965 *Phys. Rev. A* **137** 1467
[61] Wu Z J, Zhao E J, Xiang H P, Hao X F, Liu X J and Meng J 2007 *Phys.Rev. B* **76** 054115
[62] Kumar V and Tripathy S K 2014 *Journal of Alloys Compounds* **582** 101–7
[63] Mahmood T, Cao C, Tahir M, Idrees F, Ahmed M, Tanveer M, Aslam I, Usman Z, Ali Z and Hussain S 2012 *Physica B* **407** 958–65
[64] Fritz I J 1974 *J. Phys. Chem. Solids* **35** 35–817
[65] Isaak D G, Carnes J D, Anderson O I, Cynn H and Hake E 1998 *Phys Chem Miner.* **26** 31
[66] Manghnani M H, Fisher E S and Brower W S 1972 *J.PhysChem Solids* **53** 2149
[67] Reuss Von A 1929 *Z. Angew Math. Mech.* **9** 49–58
[68] Voight W 1928 Lehrbuch der Kristallphysik: verlag und Druck Von B G *Teubner in Leipzig und Berlin* **9** 62
[69] Hill R 1952 *Proc. Phys. Soc* 65, 349
[70] Chen X Q, Niu H, Li D and Li Y 2011 *Intermettalics* **19** 1275
[71] Bannikov V V, Shein I R and Ivanovskii A L 2007 *Phys. Stat. Sol.* **3** 89
[72] Fu H, Li D, Peng F, Gao T and Cheng X 2008 *Comp. Mat. Sci.* **44** 774
[73] Caravaca M A, Mino J C, Perez V J, Casali R A and Ponce C A 2009 *J. Phys.: Condens. Matter* **21** 1
[74] AI-Khatatbeh Y, Lee K K M and Kiefer B 2009 *Phys Rev B* **79** 134114
[75] Ming L C and Manghnam M H 1979 *J. Geophys. Resa* **84** 4777